Journal of Energy Chemistry 88 (2024) 144–153

Contents lists available at ScienceDirect

Journal of Energy Chemistry

journal homepage: www.elsevier.com/locate/jechem

http://www.journals.elsevier.com/journal-of-energy-chemistry/

Aqueous electrochemical delithiation of cathode materials as a strategy to selectively recover lithium from waste lithium-ion batteries

Pier Giorgio Schiavi *, Andrea Giacomo Marrani, Olga Russina, Ludovica D'Annibale, Francesco Amato, Francesca Pagnanelli, Pietro Altimari

Department of Chemistry, Sapienza University of Rome, Piazzale Aldo Moro n.5, 00185 Rome, Italy

ARTICLE INFO

Article history:
Received 17 August 2023
Revised 19 September 2023
Accepted 26 September 2023
Available online 13 October 2023

Keywords:
Lithium recovery
Lithium-ion batteries recycling
Electrochemical lithium extraction
Lithium selective
Extraction

ABSTRACT

Lithium recovery from end-of-life Li-ion batteries (LIBs) through pyro- and hydrometallurgical recycling processes involves several refining stages, with high consumption of reagents and energy. A competitive technological alternative is the electrochemical oxidation of the cathode materials, whereby lithium can be deintercalated and transferred to an electrolyte solution without the aid of chemical extracting compounds. This article investigates the potential to selectively recover Li from LIB cathode materials by direct electrochemical extraction in aqueous solutions. The process allowed to recovering up to 98% of Li from high-purity commercial cathode materials ($LiMn_2O_4$, $LiCoO_2$, and $LiNi_{1/3}Mn_{1/3}Co_{1/3}O_2$) with a faradaic efficiency of 98% and negligible co-extraction of Co, Ni, and Mn. The process was then applied to recover Li from the real waste LIBs black mass obtained by the physical treatment of electric vehicle battery packs. This black mass contained graphite, conductive carbon, and metal impurities from current collectors and steel cases, which significantly influenced the evolution and performances of Li electrochemical extraction. Particularly, due to concomitant oxidation of impurities, lithium extraction yields and faradaic efficiencies were lower than those obtained with high-purity cathode materials. Copper oxidation was found to occur within the voltage range investigated, but it could not quantitatively explain the reduced Li extraction performances. In fact, a detailed investigation revealed that above 1.3 V vs. Ag/AgCl, conductive carbon can be oxidized, contributing to the decreased Li extraction. Based on the reported experimental results, guidelines were provided that quantitatively enable the extraction of Li from the black mass, while preventing the simultaneous oxidation of impurities and, consequently, reducing the energy consumption of the proposed Li recovery method.

1. Introduction

Li-ion batteries (LIBs) play a crucial role in energy storage for various applications such as portable electronics, electric vehicles, and the storage of energy generated from renewable sources [1]. Typically, Li-ion batteries consist of 20–25 wt% of cathode material (composed of Li, Ni, Mn, and Co), followed by 20 wt% of graphite [2,3]. The remaining weight comprises the outer steel or Al case, collectors (Cu for the anode material and Al for the cathode material) on which the electrodes are deposited, separators, electrolytes, binder, and the solvents in which the electrolytes are dissolved [4]. To alleviate resource consumption and mitigate supply chain risks linked to LIBs production, it is essential to recycle end-of-life (EoL) LIBs to recover their key components. Pyrometallurgical technologies for spent LIBs recycling can be mainly divided, depending on the operating temperature, in smelting and roasting/calcination. The former uses high temperatures, above the melting point of LIB cathode materials, resulting in a challenging recovery of Li, since it remains in the slag after smelting of the batteries [4]. Roasting/calcination seems to be the most appropriate thermal treatment for the recovery of Li from spent LIBs. In particular, carbothermal reduction roasting using reducing agents (coke, carbon, and graphite) could be successfully applied to destroy the LIBs cathode materials structure with reduction of Co, Ni, and Mn to lower oxidation state and formation of Li_2O. This way allows for the recovery of lithium by simple water leaching of the resulting solid [5]. On the other hand, this apparently facile approach can be successfully applied only when almost pure LIBs cathode materials are treated. In real applications, when spent LIBs

* Corresponding author.
E-mail address: piergiorgio.schiavi@uniroma1.it (P.G. Schiavi).

https://doi.org/10.1016/j.jechem.2023.09.040

are treated, other water-soluble battery components could hinder the formation of high purity salts for the recovery of lithium. In addition, the graphite contained in spent LIBs, that can potentially be reused as anode material, is further consumed as reducing agent during the carbothermal reduction [6].

Hydrometallurgical processes for the recovery of Li rely on the dissolution of LIBs cathode materials in aqueous solution by using mineral or organic acidic solutions and reducing agents [7]. In this way, lithium is simultaneously extracted in aqueous solution together with Co, Ni, Mn, other metal impurities (Cu, Al, and Fe), battery electrolyte, and its decomposition products. Following this approach, Li is generally recovered from the residual solution after precipitation of all the transition metals in which all the chemicals used throughout the whole recycling process are still contained. This results in the recovery of Li from a Na-rich solution, due to NaOH used to recover the transition metals as low soluble salts, while Li is present at low concentration. The high solubility of Na and Li salts makes their separation challenging [8], which requires energy-consuming concentration, purification procedures, and addition of further reagents [9].

Electrochemical methods to recycle spent LIBs can be configured as a promising green alternative to the above descripted conventional recycling routes. If the electricity required for the process is produced from renewable sources, the resulting electrometallurgical process can be considered more sustainable and greener compared to the hydro- and pyrometallurgical approaches [10]. In the last years, electrochemical methods for the recycling of spent LIBs were developed covering almost all the recycling process steps. Spent LIBs electrodes were used in water electrolysis experiments in order to separate the copper and aluminium of the current collectors from the anode and cathode active materials. The detachment of the active materials is aided by different processes occurring when the spent electrodes are directly used in electrolysis experiments, such as evolution of oxygen or hydrogen gas bubbles, pH variation at the electrodes surface, and redox reactions [11–13]. Electrochemical leaching was tested as an alternative strategy with respect to hydrometallurgical metal extraction [14] and it was reported that high leaching rates can be attained when combined with heat treatment. In this way, metals can be electrochemically reduced, making their leaching easier without the application of reducing agents [15]. Selective recovery of leached metals can be attained by their electrodeposition onto the cathode during electrolysis experiments by tuning pH, electrolyte composition, and current density. Selective electrodeposition of metal impurities (i.e., Cu) with similar precipitation pH was conducted in order to purify the leachate prior to recover Ni, Mn, and Co [16]. Selective Li extraction by electrochemical methods was also recently investigated by replicating the charging mechanism of cathode material in aqueous solution. To date, the research efforts mainly focused on Li recovery from $LiFePO_4$ [17,18], while just few works regard $LiMn_2O_4$ [19], $LiNi_aMn_bCo_cO_2$ ($a + b + c = 1$) [1,14] and $LiCoO_2$ [20]. Moreover, for refs. [1,14] the aim was to produce water oxidation catalysts without considering the faradic or current efficiency required for delithiation. Remarkably, all the reported works in the literature apply this Li recovery method onto almost pure cathode materials without considering the complexity of a EoL LIBs black mass coming from a real waste. In fact, depending on the mechanical pre-treatment, the black mass will contain metals impurities (Cu, Al, and Fe), graphite, and conductive carbon that could lead to a loss in faradaic efficiency. Generally, the main scope of the reported works is the maximization of Li extraction yield, that must be underlined, but parasitic reactions possibly occurring along with delithiation should be carefully evaluated in the view of energy consumption minimization and purity of recovered Li.

In this work, the delithiation mechanism in aqueous electrolyte was firstly investigated on different commercial cathode materials. In particular, the delithiation degree (i.e., lithium extraction yield) and faradaic efficiency were evaluated along with the change of the crystal structure and the surface chemical composition. Aqueous delithiation was then applied on a EoL LIBs black mass coming from the mechanical pre-treatment of electric vehicle LIB packs. Li extraction yield and faradaic efficiency were evaluated considering the role of all black mass components including Cu, Fe, Al, graphite, and conductive carbon during delithiation. The proposed method for lithium recovery should be viewed as a pre-treatment step for recycling the black mass of LIBs, conducted prior to the recovery of other valuable metals such as Co, Ni, and Mn. This approach allows for the selective extraction, concentration, and recovery of high-purity lithium avoiding the complex separation of Li from the residual solution attained at the end of the hydrometallurgical process.

2. Experimental

2.1. Delithiation experiments

$LiCoO_2$ (Aldrich, 99.8%), $LiNi_{1/3}Mn_{1/3}Co_{1/3}O_2$ (Aldrich, >98%, particle size <0.5 μm), and $LiMn_2O_4$ (Aldrich,>99%, particle size <0.5 μm) were used as commercial cathode materials. EoL LIBs black mass was supplied by TES-Recupyl SAS (Domene, France) and obtained after crushing and sieving electric vehicles battery packs. Prior to its application in the electrochemical experiments, the received black mass was washed in water at 50 °C for 6 h in order to remove soluble Li-salts, whose dissolution during the electrochemical extraction tests would lead to overestimate the faradaic efficiency of cathode delithiation. In this way, 13% of Li, attributable to soluble electrolyte and its decomposition products, was removed. Black mass was characterized by atomic absorption spectroscopy (AAS, ContrAA300 Analytic Jena GBH) and inductively coupled plasma emission spectroscopy (ICP, Avio 220 MAX PerkinElmer Inc.) after microwave assisted digestion (Milestone ETHOS 900 - Milestone srl) of 12 samples of 0.25 g in 4 mL HCl (37% VWR Chemicals), 4 mL HNO_3 (65%, Carlo Erba Reagents), and 2 mL H_2O_2 (30%, Sigma-Aldrich). Black mass composition is reported in Table 1.

Electrochemical experiments were carried out in a jacketed three-electrode cell connected to an IVIUMnSTAT potentiostat. All the experiments were carried out at 25 ± 0.2 °C. Working electrodes were obtained by mixing the selected commercial cathode material, conductive carbon black (carbon black Super P conductive Alfa Aesar 99%), and polyvinylidene fluoride (PVDF, Alfa Aesar). The mixture was prepared as a slurry in *N*-methylpyrrolidone (NMP, Sigma-Aldrich 99%) in a weight ratio of 8:1:1. In case of application of the LIBs real waste, the slurries were obtained by mixing the powder and PVDF in a weight ratio of 9:1. The slurries were drop casted onto titanium with foils (Alfa Aesar 99.5%, annealed, thickness 0.25 mm) with active surface area

Table 1
Black mass composition.

Metal	Average (mg/g)	st.dev. (mg/g)
Co	75	3
Ni	92	1
Mn	88	6
Li	31	1
Al	6	5
Cu	13	1
Fe	1	0.2

3×3 cm^2 to obtain a mass loading of about 30 mg in any working electrodes. A graphite foil (99.8% Alfa Assar) was used as a counter-electrode and a Ag/AgCl electrode (Ag/AgCl 3 M KCl, Amel Instruments) as reference. All the potential values reported throughout the manuscript were referred to Ag/AgCl unless specified otherwise. 0.1 M Li_2SO_4 (Alfa Aesar, anhydrous, 99.7%) was used as electrolyte.

Cyclic voltammetries were carried out by using the above-described electrochemical configuration starting from the open cell voltage (OCV) with a scan rate of 0.1 mV/s. Potentiostatic delithiations were carried out at 1.5 and 2 V. Duration of delithiation experiments was defined by total charge passing during the experiments. The minimum theoretical charge required for the complete delithiation of the cathode materials was determined by the Faraday law. Experiments were then performed with total charge values of 0, 20%, 100%, and 200% in excess with respect to the computed theoretical value (see Supporting Information). The lithium extraction yield was computed starting from the metal concentrations obtained after mineralization of the electrodes at the end of any delithiation experiments Li and metal impurities extraction yields were computed as reported in the Supporting Information.

2.2. Physical-chemical characterization

The difference in the phase composition between the pristine and delithiated cathode materials was investigated through X-ray diffractometer (XRD, Bruker D8 ADVANCE) with a molybdenum anode ($K_{\alpha 1}$ = 0.709319 Å), scanning the 2theta range between 4° and 45°. The diffraction data were collected at ambient conditions in Brentano Bragg geometry, depositing the powder samples on a quartz plate. The crystal structure analysis of the samples was performed using the GISAS II program. To facilitate the comparison of the experimental data with the literature, they were converted with respect to a Cu radiation with K_α = 1.54056. Surface atomic composition variations were investigated by X-ray photoelectron spectroscopy (XPS). XPS spectra were recorded using a modified Omicron NanoTechnology MXPS system equipped with a monochromatic (Omicron XM-1000) and a twin anode (Omicron DAR-400) X-ray source, with an Omicron EA-125 energy analyser. The exciting radiation used was Al K_α ($h\upsilon$ = 1486.7 eV), generated operating the anode at 14–15 kV and 10–20 mA. All photoionization regions were acquired using an analyser pass energy of 20 eV, except for the survey scan, taken at 50 eV pass energy. Take-off angles (θ) of 11° with respect to the sample surface normal were adopted. The measurements were performed at room temperature, and the base pressure in the analyser chamber was about 2×10^{-9} mbar. The C 1*s* binding energy (BE) of the aromatic C=C bonds belonging to the graphitic component of Super P carbon of the cathodes was used as an internal standard reference at 284.2 eV for the BE scale (accuracy of ±0.05 eV). Experimental data were fitted using a Shirley or a linear function to reproduce the secondary electrons' background and pseudo-Voigt functions for the elastic peaks. These curves are described by a common set of parameters (position, full width at half maximum (FWHM), and Gaussian-Lorentzian ratio) which were let free to vary within narrow limits. Raman spectra were collected at room temperature in backscattering geometry with an inVia Renishaw micro-Raman spectrometer equipped with an air-cooled charge coupled device (CCD) detector and super-Notch filters. An Ar + ion laser (λ(laser) = 514 nm) was used, coupled to a Leica DLML microscope with a 20× objective. The resolution was 2 cm^{-1} and spectra were calibrated using the 520.5 cm^{-1} line of a silicon wafer. Infrared spectra were recorded on a Varian FT-IR 660 instrument in the range of 4000–200 cm^{-1} with a spectral resolution of 4 cm^{-1} and 64 scans in KBr pellets. Field emission scanning electron microscopy (SEM, Zeiss Auriga) was employed to characterize the morphology and size of electrodes.

3. Results and discussion

3.1. $LiMn_2O_4$

The linear sweep voltammetry of $LiMn_2O_4$ (Fig. 1a) displays two oxidation peaks, located at 0.75 and 0.88 V, corresponding to the two-step Li extraction process of $LiMn_2O_4$. Initially, lithium is removed (0.75 and 3.99 V vs. Li/Li$^+$) from the tetrahedral sites where Li-Li repulsion occurs. Subsequently, lithium ions are removed (0.88 and 4.13 V vs. Li/Li$^+$) from other tetrahedral sites where they are free from nearest neighbor interactions, thus requiring more energy [21,22]. Potentiostatic delithiations were conducted to quantify the lithium extraction yield achieved through the electrochemical oxidation of cathode materials in an aqueous electrolyte. The role of applied potential and charge was evaluated for all cathode materials by comparing the molar ratio between Li and transition metals (Co, Ni, and Mn) before and after delithiation (Eq. (S1)). A maximum Li extraction yield of 95% for $LiMn_2O_4$ was found at 2 V, with the theoretical amount of charge required for the complete extraction of Li corresponding to a faradaic efficiency of 95% (Fig. 1b). Surprisingly, a slight decrease in the Li extraction yield to 85% was observed when a charge equal to 200% of minimum theoretical charge was used (Fig. 1b). A possible explanation for this result is that, during Li extraction, the Mn species contained as Mn^{3+} in $LiMn_2O_4$ are progressively oxidized to Mn^{4+}, and formation of λ-MnO_2 could occur when Li is completely extracted. λ-MnO_2, can adsorb Li^+ through ion exchange between H^+ and Li^+ at a non-acidic pH [23], as in our experimental conditions, and it could therefore adsorb back the Li in a late stage of the experiment. In fact, it should be noted that at the working electrode the oxidation of Mn mainly occurs, while at the counter electrode the redox reactions involve reduction of protons and water leading to an increase of pH up to 10 at the end of delithiation, when the experiment is carried out at 200% charge excess. The occurred delithiation and the presence of Mn^{4+} species at the end of the process were confirmed using XPS. Fig. 1(c) shows the Li 1*s* (close to Mn 3*p*) photoionization region before and after the delithiation process. Due to the inherently low photoionization cross-section of Li core electrons in the XPS regime, the intensity of the Li 1*s* feature is generally very low. However, in all samples, a peak at 53.8 eV binding energy can be observed. This binding energy position is compatible with cationic Li intercalated within the oxide host matrix [24–26].

After the delithiation process, a drastic decrease in Li signal intensity can be observed, supporting the effectiveness of electrochemical deintercalation. In Fig. 1(d), the Mn 3*s* region is presented for both the pristine and delithiated state of $LiMn_2O_4$. In this case, the core-valence exchange coupling results in a doublet according to the spin state of the 3*s* core–hole, whose splitting energy, ΔE_{3s}, scales with the number of unpaired valence electrons, allowing for a direct assignment of the mean oxidation state [27–30]. In this case, ΔE_{3s} changes from 4.90 to 4.75 eV, from pristine to delithiated state, roughly corresponding to Mn^{3+}:Mn^{4+} percentage ratios of 50:50 (mean oxidation state + 3.5) and 35:65 (mean oxidation state + 3.65), respectively. The value found for the pristine material is in perfect coherence with literature data [24,27]. The result obtained from Mn 3*s* was then used to interpret the Mn 2*p* spectra via curve-fitting deconvolution (Fig. 1e), using the calculated free-ion multiplet structure reported by Gupta and Sen [31,32] and already used by Biesenger et al. [33] on pure transition metal oxides and hydroxides. The applied envelopes of ionized final state peaks for Mn^{3+} and Mn^{4+} correctly reproduce the Mn 2*p* experi-

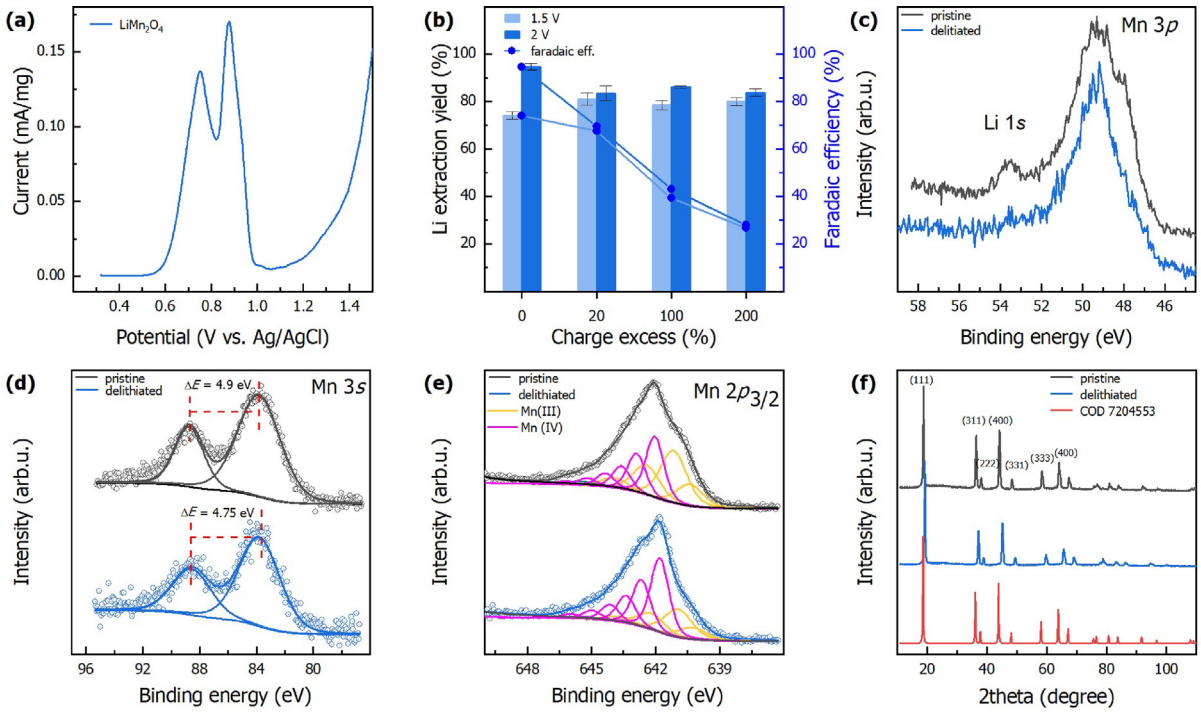

Fig. 1. (a) Linear sweep voltammetry from OCV to 1.5 V at 0.1 mV/s of $LiMn_2O_4$ (b) Lithium extraction yields and faradaic efficiency (blue dots and lines) obtained by potentiostatic delithiation. (c) Li 1*s* XPS spectra including the Mn 3*p* signal. (d) Mn 3*s* XPS spectra with core-valence coupling energy splitting (ΔE). (e) Mn 2*p* XPS spectra including Mn^{3+} and Mn^{4+} ionized final state envelopes. (f) XRD pattern including the calculated pattern for the COD 7204453 phase.

mental data according to the oxidation state ratios found via Mn 3*s* deconvolution, therefore supporting the observed change in oxidation state [34–37]. Fig. 1(f) shows the diffraction patterns obtained from the $LiMn_2O_4$ samples before and after delithiation. Both patterns are identified as a single cubic phase *Fd*-3*m* (COD 7204553). The cell parameter of the pristine sample is only slightly less than the cubic length of used phase: 8.232 Å instead of 8.244 Å. After delithiation, peaks shift to smaller angles, indicating further shrinking of the unit cell and change of the volume from 558 $Å^3$ down to 523 $Å^3$ with a cubic length of 8.055 Å. However, the single-phase crystal structure of the pristine sample is preserved in delithiated sample.

3.2. $LiCoO_2$

The $LiCoO_2$ voltammogram (Fig. 2a) displays a main peak at 0.72 V (3.97 V vs. Li/Li^+), corresponding to the extraction of Li after the oxidation of Co^{3+} to Co^{4+}. During potentiostatic delithiation, the Li extraction yield with $LiCoO_2$ increases as the applied potential and/or the charge is increased, reaching a maximum extraction yield of 97% with 20% charge excess, corresponding to about 80% faradaic efficiency. XPS measurements confirm the delithiation; in fact, the Li component in the Li 1*s* region (close to Co 3*p*, Fig. 2c) disappears. Fig. 2(d) shows the Co $2p_{3/2}$ region, where the oxidation state of Co can be evaluated prior and after delithiation. In pristine $LiCoO_2$, a main component appears at 780.0 eV (Fig. 2d magenta curve), attributable to Co^{3+} species in octahedral sites, followed by a minor component at 781.1 eV (Fig. 2d blue curve) due to a fraction of Co^{2+} in tetrahedral sites [25,26,38–41]. Further, very low-intensity features are detected at higher binding energy, associated to satellite peaks of main lines [40,41]. The overall lineshape of Co 2*p* spectrum from pristine $LiCoO_2$ is fully compatible with literature data. Upon delithiation (see lower spectrum in Fig. 2d), a slight broadening of the Co $2p_{3/2}$ signal can be detected, which can be accounted for including an additional component at low binding energy side of the spectrum (Fig. 2d green curve). This feature is similar to that reported for Li-deintercalated $LiCoO_2$ [42] and for high oxidation state cobalt compounds [43], which point at a mixed CoO_2/oxyhydroxide species. This hypothesis is supported by the comparison of O 1*s* spectra (Fig. 2e), where an increase of the –OH related feature at 532.0 eV is recorded in the delithiated sample (Fig. 2e red spectrum) at the expenses of the lattice O^{2-} contribution at 529.6 eV [20]. As a confirmation, XRD analysis indicates that after delithiation, there is a loss in the $LiCoO_2$ crystalline phase. Fig. 2(f) shows the diffraction patterns of $LiCoO_2$ samples before and after delithiation. The pristine sample is identified as a single-phase hexagonal *R*-3*m* structure (with a = 2.815 Å, c = 14.0516 Å, and volume 96.43 $Å^3$ (COD 4505482)), whereas the diffraction pattern of the delithiated sample is more complicated and cannot be solely explained in terms of changes in cell parameters. Merging XPS and XRD results, the formation of a new phase after delithiation can be inferred. In fact, after the extraction of Li from $LiCoO_2$, all the cobalt species were likely converted to Co^{4+} with the formation of CoO_2. CoO_2 is not stable in the adopted experimental conditions and can be spontaneously reduced to Co^{3+} in the presence of water and moisture, leading to the formation of CoOOH [20] as follows

$$4CoO_2 + 2H_2O \rightarrow 4CoOOH + O_2 \quad (1)$$

3.3. $LiNi_{1/3}Co_{1/3}Mn_{1/3}O_2$

The linear sweep voltammetry of $LiNi_{1/3}Co_{1/3}Mn_{1/3}O_2$ (Fig. 3a) revealed the presence of two oxidation peaks at 0.52 V (3.77 V vs. Li/Li^+) and 1.15 V (4.39 vs. Li/Li^+), corresponding to the redox couples Ni^{2+}/N^{i4+} and Co^{3+}/Co^{4+}, respectively. As expected, the Co^{3+}/Co^{4+}oxidation potential in $LiNi_{1/3}Co_{1/3}Mn_{1/3}O_2$ shifts to a higher value compared to $LiCoO_2$. Similar results were reported in mixed metal cathode materials where low potential oxidations are related to the extraction of 2/3 of the Li atoms (1/3 related to

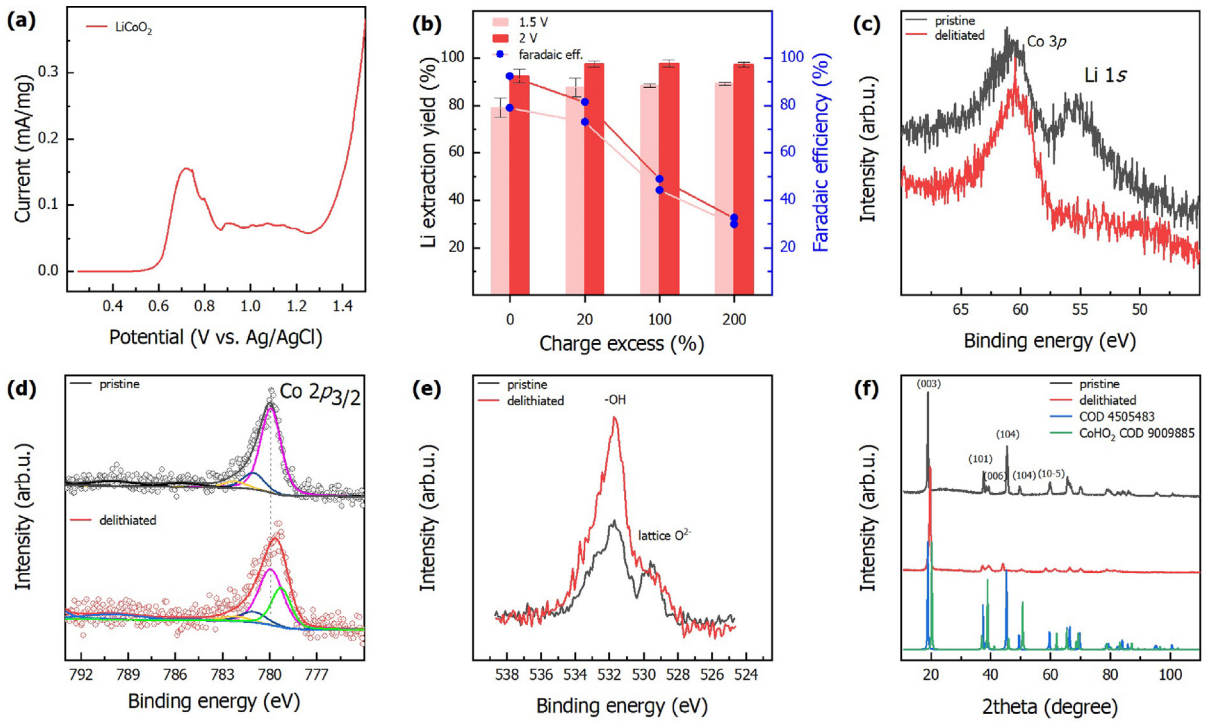

Fig. 2. (a) Linear sweep voltammetry from OCV to 1.5 V at 0.1 mV/s of $LiCoO_2$. (b) Lithium extraction yields and faradaic efficiency (blue dots and lines) obtained by potentiostatic delithiation. (c) Li 1*s* XPS spectra including the Co 3*p* signal. (d) Co $2p_{3/2}$ and (e) O 1*s* XPS spectra normalized with respect to the low energy lattice O^{2-} contribution. (f) XRD of $LiCoO_2$ before and after de-lithiation. The blue line represents the calculated XRD pattern for the phase with hexagonal *R*-3*m* structure (COD 4505482). The green line is XRD calculated for the $CoHO_2$ hexagonal *R*-3*m* structure (COD 9009884).

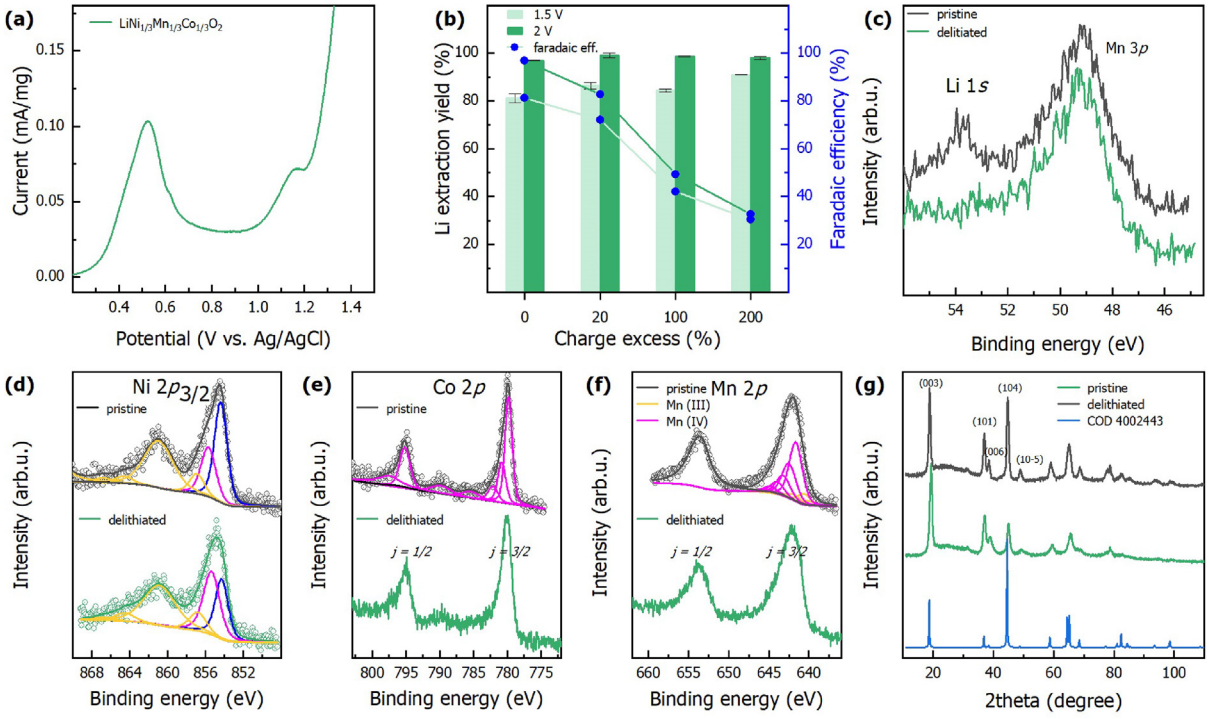

Fig. 3. (a) Linear sweep voltammetry from OCV to 1.5 V at 0.1 mV/s of $LiNi_{1/3}Mn_{1/3}Co_{1/3}O_2$. (b) Lithium extraction yields and faradaic efficiency (blue dots and lines) obtained by potentistatic delithiation. (c) Li 1*s* XPS spectra including the Mn 3*p* signal. (d) Ni $2p_{3/2}$, (e) Co 2*p*, and (f) Mn 2*p* XPS spectra. (g) XRD pattern of commercial $Li_{1-x}Ni_{1/3}Co_{1/3}Mn_{1/3}O_2$ samples.

Ni^{2+}/Ni^{3+} and 1/3 related to Ni^{3+}/Ni^{4+}), and the remaining Li is completely extracted at a higher potential, accompanied by the oxidation of Co^{3+}/Co^{4+} [44,45]. Potentiostatic delithiation (Fig. 3b) allowed for a Li extraction yield of up to 98% with the theoretical amount of charge, implying a faradaic efficiency of 98% at an applied potential of 2 V. Since Li was almost completely extracted

with the theoretical amount of charge, increasing the charge (duration) of delithiation did not result in a significant variation in the extraction yield but it only decreased the faradaic efficiency. Effective delithiation was confirmed by XPS measurements, showing the absence of Li 1*s* signal (Fig. 3c) after delithiation. The Ni $2p_{3/2}$ XPS spectrum (Fig. 3d) of pristine $LiNi_{1/3}Co_{1/3}Mn_{1/3}O_2$ sample shows the typical multiplet of ionized final state of Ni^{2+} within an octahedral oxide coordination environment, with the main component at low BE (Fig. 3d blue curve) located at 854.3 eV attributed to the 2*p* core–hole screened by the surrounding ligands ($2p^{-1}_{3/2}3d^9\underline{L}^{-1}$) [46–51]. Detailed assignment of the other peaks can be found elsewhere [46–51]. It is worth mentioning that on passing to the delithiated state, an increase of the feature at 855.4 eV (Fig. 3d magenta curve) can be detected. This component in NiO is typically attributed to a non-locally screened Ni^{2+} 2*p* core–hole [46–49], but some authors have shown that Ni^{3+} species may display Ni 2*p* ionization features around this binding energy [52–54]. Therefore, such an enhancement of this component is here associated to an increase of oxidation state of Ni upon delithiation. As to the Co 2*p* spectrum (Fig. 3e), it shows the predominant feature of Co^{3+} at 779.8 eV, with a minor component of Co^{2+} at 780.9 eV, while the other three small features are Co^{3+} and Co^{2+} satellites. The overall lineshape is perfectly coherent with literature data on $LiNi_{1/3}Co_{1/3}Mn_{1/3}O_2$ electrodes [25,34,38–41,55,56]. The comparison between the pristine and delithiated samples does not show any change in the lineshape of Co 2*p*, suggesting that a possible transformation of Co^{3+} into Co^{4+} driven by delithiation is only transient, with a probable subsequent spontaneous reduction back to Co^{3+}. As to Mn, this being, as expected, electrochemically inactive, the Mn 2*p* XPS spectra (Fig. 3f) resulted nearly identical prior and after delithiation, with a predominant contribution from Mn^{4+} (Fig. 3f magenta envelope of curves), as supported by a ΔE_{3s} value of 4.6 eV [25,57]. Fig. 3(g) contains the XRD diffraction patterns of commercial $LiNi_{1/3}Co_{1/3}Mn_{1/3}O_2$ before and after delithiation. Both patterns could be identified as a single trigonal (hexagonal axes) *R*-3*m*:*H* (166) phase. The phase COD 4002443 cell parameters are a = 2.86 Å and c = 14.227 Å. However, all peaks in our experimental data slightly shift towards larger angles comparing to the phase structure, indicating a smaller cell compared with the reference pattern. Using the GISAS-II fits of experimental diffraction patterns we obtained a = 2.87 Å and c = 14.05 Å for the pristine sample, while a = 2.858 Å and c = 14.186 Å for the delithiated one. The decrease of the a value after delithiation is due to Li removal from the layered structure of $LiNi_{1/3}Co_{1/3}Mn_{1/3}O_2$. The increase in c length upon delithiation is reflected in the shift of the (003) peak to the smallest 2theta value: in the initial sample it is at 2theta of 8.63°, after delithiation it moves to 8.83°.

3.4. EoL LIBs black mass

As shown in Table 1, Co, Ni, and Mn in EoL LIBs black mass are present in the same molar ratio, and the XRD pattern of the black mass can therefore be indexed to partially delithiated $LiNi_{1/3}Co_{1/3}Mn_{1/3}O_2$ (Fig. 4f). The recorded voltammogram (Fig. 4a) displays a broad peak at around 0.9 V, which should be associated with the oxidation of $LiNi_{1/3}Co_{1/3}Mn_{1/3}O_2$. However, when compared to the voltammogram of commercial $LiNi_{1/3}Co_{1/3}Mn_{1/3}O_2$ (Fig. 3a), the peak shifts to higher potential values. Similar results were also observed for cycled $LiNi_{1/3}Co_{1/3}Mn_{1/3}O_2$, where generally the oxidation peak shifts to higher potentials during cycling [58]. This suggests that the cathode materials in the black mass from waste LIBs have undergone charge/discharge cycles, leading to a loss in the initial Li storage capacity, and the consequent shift in the oxidation potential to higher values is linked to the higher oxidation state of metals compared to the pristine cathode material. As a confirmation, XPS measurements (Fig. S1) indicated the presence of Ni^{3+} (main Ni 2*p* component at 855.6 eV) in the EoL LIBs black mass before delithiation, instead of the expected Ni^{2+} for pristine $LiNi_{1/3}Co_{1/3}Mn_{1/3}O_2$. At the same time, no XPS spectral variations were found for Co and Mn prior and after delithiation (Figs. S2 and S3). This finding calls for a partial delithiation of the pristine cathode material of the EoL LIBs black mass, since the absence of Li^+ must be accompanied by the oxidation of metals to ensure the neutrality of the oxide ($Li_{1-x}(Ni_{1/3}Co_{1/3}Mn_{1/3})^{ox.state+x}O_2$). Interestingly, for all tested materials, the extraction of Li could be performed without reaching potentials causing the oxidation of water, which could be detrimental to the recovery of Li as well as to the commercial cathode materials. In fact, water oxidation could result in a local decrease in pH ($H_2O \rightarrow \frac{1}{2}O_2 + 2H^+ + 2e^-$) on the battery material surface, leading to the dissolution of the LIBs metal oxide [59,60] into the Li-rich solution, compromising the purity of the finally recovered Li. Notably, the electrochemical characterization of the LIBs waste (Fig. 4a) reveals a peak at a low potential value of 0.25 V, which can be attributed to the oxidation of metallic copper. As indicated in Table 1, the EoL LIBs black mass contains about 13 mg/g of copper originating from the graphite current collector. Consequently, at the potential required for the oxidation of cathode materials and Li extraction, the simultaneous oxidation of copper could occur, compromising the purity of the recovered lithium. However, no associated peaks related to other metallic impurities (Fe and Al) were detected. Potentiostatic delithiation of the LIBs black mass demonstrated lower Li extraction yields compared to commercial cathode materials and, particularly, $LiNi_{1/3}Co_{1/3}Mn_{1/3}O_2$. Specifically, the Li extraction yield was approximately 70% with the theoretical amount of charge, reaching 83% with a 200% charge excess (Fig. 4b). This decreased Li extraction yield may be explained by the concomitant electrochemical oxidation of metal impurities. Because of these additional faradaic processes, the charge required to attain complete Li extraction may be significantly larger than that necessary to achieve the delithiation of pure cathode materials. In order to verify this hypothesis, the electrochemical oxidation and extraction of metal impurities (Cu, Al, and Fe) was investigated. Fig. 4(c) shows that the Cu extraction yield attained during Li extraction was about 80%. The Cu extraction was generally higher at the lower applied potential of 1.5 V, which can be explained by remarking that the potential to oxidize Cu is lower than that required to oxidize the cathode materials in EoL LIBs black mass. Al extraction yields did not show a specific trend (Fig. S4), and the extraction yield associated errors are high due to the heterogeneity of Al distribution in the black mass (6 ± 5 mg/g Table 1). The higher extraction yield attained was 40% at 2 V and 200% charge excess. Since (i) no oxidation peak/current associated with Al was found in the voltammetry, (ii) Al oxidation produces insoluble Al_2O_3 in the solid phase, and (iii) Al has amphoteric behaviour, we cannot exclude that its extraction is induced by the increase of pH during the delithiation. In fact, in all the delithiation experiments, including commercial materials, pH at the end of delithiation increases from about 7 up to 10, due to water reduction at the counter electrode. It should be noted that the removal of Al impurity using NaOH solution is a common pre-treatment of LIBs black mass that could be used also in this case to avoid contamination of Li solution obtained by aqueous delithiation. Negligible extraction of Fe was found within the investigated potential range since Fe should be present as a steel alloy composing the metallic case of batteries and its initial concentration in black mass is only 1 mg/g. XPS measurements displayed both the absence of Li (Fig. 4d) and Cu (Fig. 4e) after delithiation, confirming their simultaneous extraction. Thus, Cu oxidation could be responsible for the lower extraction of Li in EoL LIBs black mass. On the other hand, the theoretical charge for the complete oxidation of Cu (~40 C/g) corresponds to

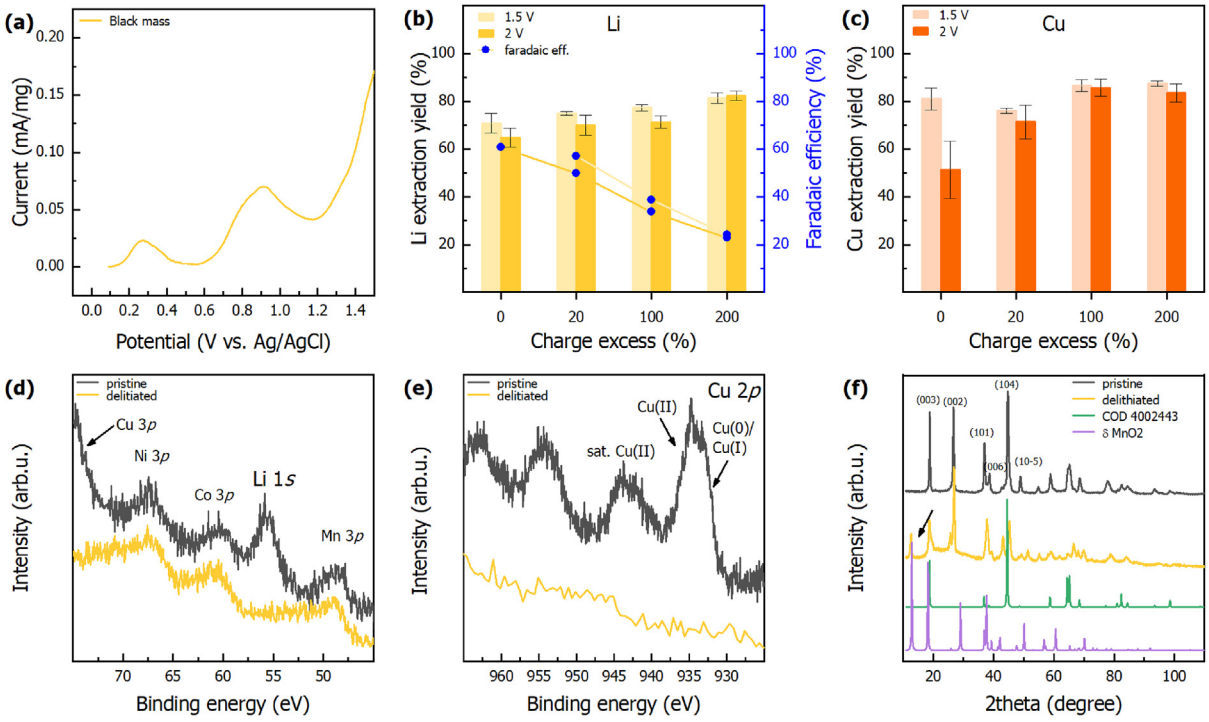

Fig. 4. (a) Linear sweep voltammetry from OCV to 1.5 V at 0.1 mV/s of EoL LIBs black mass. (b) Lithium extraction yields and faradaic efficiency (blue dots and lines) obtained by potentiostatic delithiation. (c) Cu extrtaction yields obtained during potentiostatic delitathition. (d) Li 1*s* photoionization regions including the Mn 3*p* region. (e) Cu 2*p* XPS. (f) XRD pattern of $Li_{1-x}Ni_{1/3}Co_{1/3}Mn_{1/3}O_2$ samples.

only ~9% of the theoretical charge (493 C/g) imposed for the oxidation of EoL LIBs black mass and to ~3% of the total charge in the case of 200% charge excess (1480 C/g). This suggests that Cu alone cannot explain the lower Li extraction yields found with the EoL LIBs black mass. An additional consideration about Cu impurities should be done. Cu ions released after oxidation of metallic copper can be reduced at the cathode side during the extraction of lithium. In this way, high purity copper could be recovered at the cathode side. However, if the aim is the recovery of lithium hydroxide in a two-chamber electrochemical cell, the cathode side will be at a high pH value and copper will precipitate as hydroxide, compromising the recovery of Li. It should be remarked that, as shown in Fig. 4(a), Cu oxidation occurs at a lower potential (0.15 V) with respect to the oxidation of transition metals that compose the cathodes (between 0.4 and 0.6 V). This potential gap could allow for the selective oxidation of Cu prior to delithiation. Specifically, a method for the separation of Cu could include: (i) applying a potential of 0.15 V to the black mass of EoL LIBs to oxidize metallic Cu to Cu^{2+} and enable its dissolution in the electrolyte, (ii) once all the Cu is oxidized, replacing the electrolyte solution with a new one without copper, (iii) raising the potential to facilitate the oxidation of cathode materials and the extraction of Li in a pure Li solution.

Addressing the issue of low extraction yield that cannot be justified by the oxidation of metallic impurities, it should be noted that, for EoL LIBs black mass, the Li extraction yield is higher at the lower applied potential of 1.5 V (Fig. 4b), indicating that an additional faradaic process may occur at higher potential absorbing part of the total transferred charge and preventing that it is used for the oxidation of cathode materials in EoL LIBs black mass. The XRD pattern (Fig. 4f) of delithiated EoL black mass reveals a new intense peak at low 2theta (12°) that is not present in the commercial $LiNi_{1/3}Co_{1/3}Mn_{1/3}O_2$ after delithiation. It was recently reported that for above 90% delithiation of $LiNi_{1/3}Co_{1/3}Mn_{1/3}O_2$ cathode material, the crystal structure is re-arranged with the formation of δ-MnO_2 with the appearance of the diffraction peak at 12° [1]. However, in our case after a 99% delithiation of commercial $LiNi_{1/3}Co_{1/3}Mn_{1/3}O_2$, this new crystalline phase (Fig. 3g) was not found. In addition to the presence of metallic impurities, the main difference of the EoL LIBs black mass from the tested commercial cathode materials is the graphite content. In fact, the XRD peak at a low angle could also be indexed to graphite oxide, in which graphite layers increased their inter-distance as a consequence of introduction of oxygen functionalities driven by oxidation. An additional indication of graphite oxidation could derive from the appearance of an amorphous broad peak in the XRD pattern of delithiated EoL LIBs black mass (Fig. 4f yellow line). In fact, the graphite oxidation process leads to a drastic change in the diffraction pattern: while graphite has a typical peak at 2theta 27° (002), graphite oxide is characterized by the increase of an amorphous signal and a peak at low 2theta position, typically at 11° (001) [61]. To prove the occurrence of graphite oxidation, linear sweep voltammetry was carried out using a working electrode composed of graphite and PVDF as a binder (Fig. 5a). No significative faradaic process, except water oxidation starting from 1.2 V, was observed. Additionally, XRD measurements were repeated on electrodes with the same composition (Graphite and PVDF) that were first used in potentiostatic experiments at 2 V and applying the same amount of charge used in the delithiation experiments. XRD measurements revealed the absence of the low angle peak that can be attributed to graphite oxide (Fig. S5). To further investigate the possibility of graphite oxidation, Raman and FT-IR measurements were carried out. Raman spectra (Figs. S6 and S7) display a significant increase in the I_d/I_g ratio after applying 2 V to commercial graphite electrodes, while a weak band attributable to the C–O stretching vibrations in the range between 1130 and 1170 cm^{-1} was found by FT-IR (Figs. S8 and S9). These results indicate the introduction of defects is likely associated to the formation of oxygenated functional groups at the surface of carbon. But likely, the extent of graphite oxidation is not enough to contribute to an appreciable

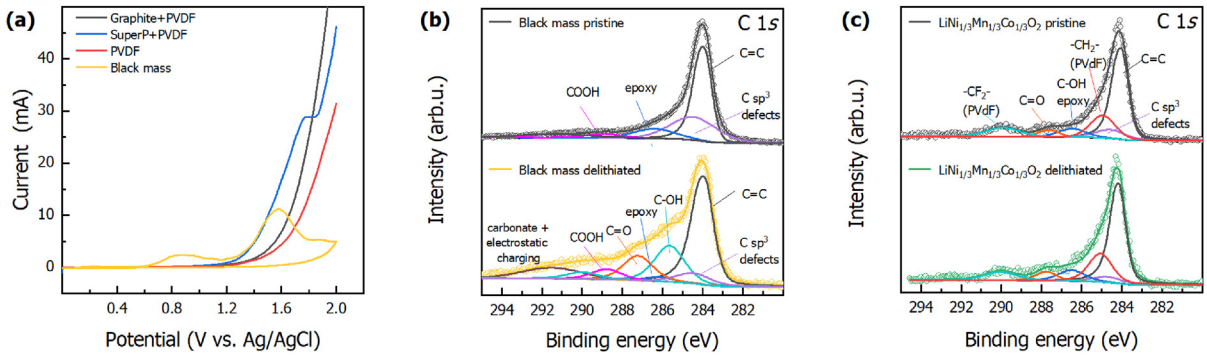

Fig. 5. (a) Linear sweep voltammetry from OCV to 2 V at 0.1 mV/s using electrodes composed by graphite, Super P conductive carbon, PVDF, and EoL LIBs black mass. C 1*s* XPS spectra for (b) $LiNi_{1/3}Co_{1/3}Mn_{1/3}O_2$ and (c) EoL LIBs black mass prior and after delithiation.

crystalline phase variation by XRD patterns. Indeed, electrochemical oxidation of graphite generally requires a higher applied potential (at least a cell potential of 5 V), and intercalated cations are added to aid its exfoliation [62,63]. However, the possibility that EoL graphite contained in the black mass can be more easily electrochemically oxidized compared to pristine commercial graphite should be considered. In fact, it was recently reported that lithiation/delithiation of graphite during LIBs cycling aids the subsequent exfoliation towards the production of graphene oxide [64–66].

Finally, the role of conductive carbon was also considered. To evaluate the electrochemical stability of conductive carbon, linear sweep voltammetry of an electrode composed by Super P:PVDF (9:1) was performed (Fig. 5a). An oxidation current starting from 1.2 V and a peak at about 1.7 V were found. The same results were found also in the EoL LIBs black mass and in the other linear sweep voltammetries of the commercial cathode materials conducted at up to 2 V (Fig. S10). It was reported that the electrochemical stability of conductive carbon in LIBs is compromised above 4.4 V vs. Li/Li^+ (1.2 V vs. Ag/AgCl), and parasitic reactions occur depending on the oxygen functional groups originally present on the carbon surface, adsorbed water, and graphitization degree. In particular, below 4.8 V vs. Li/Li^+ (1.6 V vs. Ag/AgCl), the main reactions involve carbon surface functionalization group while, above 4.8 V, intercalation of anions is the dominant reactions, especially with high graphitization degree carbon [67,68]. During potentiostatic delithiation at 2 V (5.2 V vs. Li/Li^+), all the described parasitic reactions are permitted. To evaluate the oxidation of carbon contained in EoL LIBs black mass, XPS measurements were carried out. In Fig. 5(b), C 1*s* spectra of EoL LIBs black mass prior and after the delithiation process (2 V, 200% charge excess) were reported. A prominent difference between the two samples can be seen due to the introduction of several carbon functional groups after delithiation. In particular, the C 1*s* XPS spectrum of EoL LIBs black mass prior delithiation shows the contribution of aromatic sp^2 C at 284.0 eV with a moderately extended tail at the high BE side, accounting for the presence of defective C sites (sp^3) and slightly oxidized C moieties (epoxy, –COOH) [69,70]. After delithiation, an extended oxidation of the carbon species can be detected, with an increased intensity corresponding to hydroxyl, epoxy, carbonyl, carboxyl, and carbonate groups, with a concomitant diminution of the sp^3 defective component. On the other hand, conductive carbon (Super P) was also added during the formulation of slurry for the preparation of electrodes using commercial cathode materials where almost quantitative extraction of Li was reached ($LiNi_{1/3}Co_{1/3}Mn_{1/3}O_2$). In fact, the oxidation of conductive carbon added to the $LiNi_{1/3}Co_{1/3}Mn_{1/3}O_2$ cathode materials did not undergo any oxidation, as displayed in Fig. 5(c), where the lineshapes of the two C 1*s* spectra prior and after delithiation are nearly identical. This can be explained in terms of the relative amount of cathode materials and conductive carbon in the commercial $LiNi_{1/3}Co_{1/3}Mn_{1/3}O_2$ and EoL LIBs black mass electrodes. $LiNi_{1/3}Co_{1/3}Mn_{1/3}O_2$ commercial electrodes are composed of 80% $LiNi_{1/3}Co_{1/3}Mn_{1/3}O_2$ and 10% of Super P, while, in the case of EoL LIBs black mass, Super P was not added during the formulation of slurries since conductive carbon is already present in the black mass and comes from both anode and cathode materials. Consequently, considering the composition of black mass (Table 1), the cathode material contained in the EoL LIBs black mass is ~40%, about half in comparison to the commercial cathode material, and probably with double the amount of conductive carbon (20%). Because of the lower amount of cathode materials and the higher amount of conductive carbon, in EoL LIBs black mass, the current consumed by the oxidation of conductive carbon will be higher compared to electrodes prepared by using the commercial $LiNi_{1/3}Mn_{1/3}Co_{1/3}O_2$.

To verify the ability of the method to selectively extract Li without causing the dissolution of other cathode elements, ICP analysis of the resulting electrolyte at the end of any delithiation experiment was carried out evidencing a negligible extraction of Co, Ni, and Mn (concentration lower than 0.01 mg/L, extraction lower than 0.03%). Additionally, if Co, Ni, and Mn were simultaneously extracted with Li during the potentiostatic delithiation, they would be present as divalent cations in the aqueous solution and could be reduced at the counter electrodes. Accordingly, the extraction yield of Co, Ni, and Mn determined by analysing the concentration in the electrolyte solution could be underestimated. Although the applied potential is oxidative and it is unlikely that the metals are reduced to divalent form, as confirmed by all the XPS measurements reported throughout the paper, to exclude the possibility of metals reduction to the counter electrode, in the case of EoL LIBs black mass, the digestion of the counter electrodes used during the three delithiations was performed to evaluate if Co, Ni, and Mn were electrodeposited after any triplicate of potentiostatic delithiations (same cathode material type, potential, and charge). Using this approach an extraction of 0.03% of Co, 0.05% of Ni, and 0.01% of Mn was found after ICP analysis of solution resulting from the counter electrodes digestion in the case of EoL LIBs black mass delithiations.

4. Conclusions

Aqueous electrochemical delithiation of $LiMn_2O_4$, $LiCoO_2$, and $LiNi_{1/3}Mn_{1/3}Co_{1/3}O_2$ was performed allowing to attaining Li extraction yields of 95%, 97%, and 99%, respectively. The faradaic efficiencies associated with the maximum extraction yields were 80%, 95%, and 99%, with negligible co-extraction of Co, Ni, and Mn during all the potentiostatic delithiations. As compared with the application

of commercial cathode materials, a lower Li extraction yield (80%) was observed when the electrochemical delithiation was performed by employing an EoL LIBs black mass. The influence of all the materials composing the EoL LIBs black mass on the attained Li extraction yield and faradaic efficiency was evaluated. The decreased Li extraction yields cannot be justified by the concomitant oxidation of metallic impurities, particularly Cu, due to its low amount and the associated charge required for oxidation. While electrochemical characterizations did not reveal any faradaic process involving graphite within the potential range explored in the delithiation experiments, Raman of delithiated EoL LIBS black mass and FT-IR measurements of commercial graphite could suggest a little extent of graphite oxidation along with Li extraction mainly attributable to the functionalization of amorphous surface carbon of graphite. A clear oxidative process is, in contrast, evident for Super P conductive carbon within the potential range used in the delithiation experiments. The oxidation of carbon was confirmed by comparing pristine and delithiated XPS C 1*s* spectra of EoL LIBs black mass. Several carbon functional groups were found after delithiation, corresponding to hydroxyl, epoxy, carbonyl, and carboxyl functionalization, confirming the oxidation of carbon, most likely originating from conductive carbon. Indeed, it is not possible to distinguish with certainty between the oxidation of conductive carbon and graphite contained in the EoL LIBs black mass. Nevertheless, to improve Li extraction yields and faradaic efficiency, aiming to reduce energy consumption and implement the process on a larger scale, the carbonaceous fraction should be separated from the black mass. In this view, two primary strategies can be pursued to separate the carbonaceous fraction from the black mass before the delithiation process. Specifically, graphite and conductive carbon can be removed either through froth flotation or, as an alternative, carbon can be selectively removed from graphite through thermal treatment. This latter procedure could help to definitively determine whether the oxidation of carbon is also associated with graphite and not solely with Super P conductive carbon in the case of EoL LIBs black mass. The proposed recycling idea based on the charge mechanism of LIBs cathode materials in water could be evaluated as a promising strategy for the production of green H_2 in an integrated water electrolyser adding Li as high-value product coming from the anode side where generally oxygen is produced.

Declaration of competing interest

The authors declare that they have no known competing financial interests or personal relationships that could have appeared to influence the work reported in this paper.

Acknowledgments

This work was carried out within the Horizon Europe Project "Batteries reuse and direct production of high performances cathodic and anodic materials and other raw materials from batteries recycling using low cost and environmentally friendly technologies" (RHINOCEROS project, grant no. 101069685). Views and opinions expressed within this scientific paper are however those of the authors only and do not necessarily reflect those of the European Climate, Infrastructure and Environment Executive Agency (CINEA). Neither the European Union nor the granting authority can be held responsible for them.

Appendix A. Supplementary data

Supplementary data to this article can be found online at https://doi.org/10.1016/j.jechem.2023.09.040.

References

[1] H. Lv, H. Huang, C. Huang, Q. Gao, Z. Yang, W. Zhang, Appl. Catal. B 283 (2021) 119634.
[2] M. Kotal, S. Jakhar, S. Roy, H.K. Sharma, J. Energy Storage 47 (2022) 103534.
[3] H. Zhao, W.-Y.-A. Lam, L. Sheng, L. Wang, P. Bai, Y. Yang, D. Ren, H. Xu, X. He, Adv. Energy Mater. 12 (2022) 2103894.
[4] J. Hou, X. Ma, J. Fu, P. Vanaphuti, Z. Yao, Y. Liu, Z. Yang, Y. Wang, Green Chem. 24 (2022) 7049–7060.
[5] B. Makuza, Q. Tian, X. Guo, K. Chattopadhyay, D. Yu, J. Power Sources 491 (2021) 229622.
[6] G. Zhang, X. Yuan, C.Y. Tay, Y. He, H. Wang, C. Duan, Sep. Purif. Technol. 314 (2023) 123555.
[7] K. Serbara Bejigo, K. Bhunia, J. Kim, C. Lee, S. Back, S.J. Kim, J. Energy Chem. 82 (2023) 148–157.
[8] L. Yang, Y. Tu, H. Li, W. Zhan, H. Hu, Y. Wei, C. Chen, K. Liu, P. Shao, M. Li, G. Yang, X. Luo, Angew. Chem. Int. Ed. 62 (2023) e202308702.
[9] C. Liu, J. Lin, H. Cao, Y. Zhang, Z. Sun, J. Clean. Prod. 228 (2019) 801–813.
[10] H.A. Petersen, T.H.T. Myren, S.J. O'Sullivan, O.R. Luca, Mater Adv. 2 (2021) 1113–1138.
[11] N. Cao, Y. Zhang, L. Chen, W. Chu, Y. Huang, Y. Jia, M. Wang, J. Power Sources 483 (2021) 229163.
[12] W. Chu, Y. Zhang, L. Chen, K. Wu, Y. Huang, Y. Jia, Sep. Purif. Technol. 269 (2021) 118704.
[13] K. Liu, S. Yang, F. Lai, H. Wang, Y. Huang, F. Zheng, S. Wang, X. Zhang, Q. Li, ACS Appl. Energy Mater. 3 (2020) 4767–4776.
[14] L. Yang, Z. Gao, T. Liu, M. Huang, G. Liu, Y. Feng, P. Shao, X. Luo, Environ. Sci. Tech. 57 (2023) 4591–4597.
[15] S. Lei, Y. Zhang, S. Song, R. Xu, W. Sun, S. Xu, Y. Yang, ACS Sustain. Chem. Eng. 9 (2021) 7053–7062.
[16] X. Li, S. Liu, J. Yang, Z. He, J. Zheng, Y. Li, Energy Storage Mater. 55 (2023) 606–630.
[17] L. He, Z. Li, Y. Zhu, C. Yang, ACS Sustain. Chem. Eng. 8 (2020) 15915–15926.
[18] Z. Li, D.F. Liu, J. Xiong, L. He, Z. Zhao, D. Wang, Waste Manag. 107 (2020) 1–8.
[19] Z. Li, L. He, Z.W. Zhao, D. Wang, W. Xu, ACS Sustain. Chem. Eng. 7 (2019) 16738–16746.
[20] C. Huang, H. Lv, Z. Yang, C. Lian, J. Du, G. Liu, W. Tang, Z. Xu, Z. Chi, H. Liu, H. Huang, W. Zhang, J. Mater. Chem. A Mater. 10 (2022) 3359–3372.
[21] T.F. Yi, C.L. Hao, C.B. Yue, R.S. Zhu, J. Shu, Synth. Met. 159 (2009) 1255–1260.
[22] Y. Xia, M. Yoshio, J. Electrochem. Soc. 143 (1996) 825–833.
[23] X. Luo, K. Zhang, J. Luo, S. Luo, J. Crittenden, Environ. Sci. Tech. 50 (2016) 13002–13012.
[24] M.C. Militello, S.W. Gaarenstroom, Surface Sci. Spectra. 8 (2001) 207–213.
[25] G. Cherkashinin, K. Nikolowski, H. Ehrenberg, S. Jacke, L. Dimesso, W. Jaegermann, Phys.l Chem. Chem. Phys. 14 (2012) 12321–12331.
[26] G. Cherkashinin, W. Jaegermann, The Journal of Chemical Physics 144 (2016) 184706.
[27] V.R. Galakhov, M. Demeter, S. Bartkowski, M. Neumann, N.A. Ovechkina, E.Z. Kurmaev, N.I. Lobachevskaya, Y.M. Mukovskii, J. Mitchell, D.L. Ederer, Phys. Rev. B 65 (2002) 113102.
[28] A.J. Nelson, J.G. Reynolds, J.W. Roos, J. Vacuum Sci. Technol. A 18 (2000) 1072–1076.
[29] B.D. Hermsmeier, C.S. Fadley, B. Sinkovic, M.O. Krause, J. Jimenez-Mier, P. Gerard, T.A. Carlson, S.T. Manson, S.K. Bhattacharya, Phys. Rev. B 48 (1993) 12425–12437.
[30] F. Müller, R. De Masi, D. Reinicke, P. Steiner, S. Hüfner, K. Stöwe, Surf. Sci. 520 (2002) 158–172.
[31] R.P. Gupta, S.K. Sen, Phys. Rev. B 10 (1974) 71–77.
[32] R.P. Gupta, S.K. Sen, Phys. Rev. B 12 (1975) 15–19.
[33] M.C. Biesinger, B.P. Payne, A.P. Grosvenor, L.W.M. Lau, A.R. Gerson, R.S.C. Smart, Appl. Surf. Sci. 257 (2011) 2717–2730.
[34] R. Azmi, V. Trouillet, M. Strafela, S. Ulrich, H. Ehrenberg, M. Bruns, Surf. Interface Analy. 50 (2018) 43–51.
[35] A. Quesne-Turin, G. Vallverdu, D. Flahaut, J. Allouche, L. Croguennec, M. Ménétrier, I. Baraille, ACS Appl. Mater. Interfaces 9 (2017) 44922–44930.
[36] D. Tang, Y. Sun, Z. Yang, L. Ben, L. Gu, X. Huang, Chem. Mater. 26 (2014) 3535–3543.
[37] M.A. Stranick, Surf. Sci. Spectra 6 (1999) 39–46.
[38] J. Van Elp, J.L. Wieland, H. Eskes, P. Kuiper, G.A. Sawatzky, F.M.F. De Groot, T.S. Turner, Phys. Rev. B 44 (1991) 6090–6103.
[39] Y.M. Kolotyrkin, I.D. Belova, Y.E. Roginskaya, V.B. Kozhevnikov, D.S. Zakhar'in, Y.N. Venevtsev, Mater. Chem. Phys. 11 (1984) 29–48.
[40] V.R. Galakhov, V.V. Karelina, D.G. Kellerman, V.S. Gorshkov, N.A. Ovechkina, M. Neumann, Phys. Solid State 44 (2002) 266–273.
[41] A.W. Moses, H.G.G. Flores, J.G. Kim, M.A. Langell, Appl. Surf. Sci. 253 (2007) 4782–4791.
[42] L. Dahéron, R. Dedryvère, H. Martinez, M. Ménétrier, C. Denage, C. Delmas, D. Gonbeau, Chem. Mater. 20 (2008) 583–590.
[43] A.J.U. Holt, S. Pakdel, J. Rodríguez-Fernández, Y. Zhang, D. Curcio, Z. Sun, P. Lacovig, Y.X. Yao, J. V. Lauritsen, S. Lizzit, N. Lanat, P. Hofmann, M. Bianchi, C.E. Sanders, 2D Mater. 8 (2021) 035050.
[44] N. Yabuuchi, Y. Makimura, T. Ohzuku, J. Electrochem. Soc. 154 (2007) A314.
[45] J. Choi, A. Manthiram, Electrochem. Solid-State Lett. 8 (2005) C102.
[46] J. Van Elp, H. Eskes, P. Kuiper, G.A. Sawatzky, Phys. Rev. B 45 (1992) 1612–1622.

[47] M.A. Van Veenendaal, G.A. Sawatzky, Phys. Rev. Lett. 70 (1993) 2459–2462.
[48] R.J.O. Mossanek, I. Preda, M. Abbate, J. Rubio-Zuazo, G.R. Castro, A. Vollmer, A. Gutiérrez, L. Soriano, Chem. Phys. Lett. 501 (2011) 437–441.
[49] D. Alders, G. Sawatzky, F. Voogt, T. Hibma, Physical Review BCondens Matter. Mater. Phys. 54 (1996) 7716–7719.
[50] A.G. Marrani, V. Novelli, S. Sheehan, D.P. Dowling, D. Dini, ACS Appl. Mater. Interfaces 6 (2014) 143–152.
[51] D. Giacco, T. Skála, S. Brutti, A.G. Marrani, ACS Appl. Nano Mater. 6 (2023) 10178–10190.
[52] J.F. Marco, J.R. Gancedo, M. Gracia, J.L. Gautier, E.I. Ríos, H.M. Palmer, C. Greaves, F.J. Berry, J. Mater. Chem. 11 (2001) 3087–3093.
[53] A. Thissen, D. Ensling, F.J.F. Madrigal, W. Jaegermann, R. Alcántara, P. Lavela, J. L. Tirado, Chem. Mater. 17 (2005) 5202–5208.
[54] A.F. Carley, S.D. Jackson, J.N. O'Shea, M.W. Roberts, Surf. Sci. 440 (1999) L868–L874.
[55] R.T. Haasch, D.P. Abraham, Surf. Sci. Spectra 26 (2019) 014009.
[56] R. Azmi, M. Masoumi, H. Ehrenberg, V. Trouillet, M. Bruns, Surf. Interface Analy. 50 (2018) 1132–1137.
[57] M.C. Militello, S.W. Gaarenstroom, Surf. Sci. Spectra 8 (2001) 200–206.
[58] Y. Wang, J. Luo, C. Wang, Y. Xia, J. Electrochem. Soc. 153 (2006) A1425.
[59] S. Li, X. Wu, Y. Jiang, T. Zhou, Y. Zhao, X. Chen, Waste Manag. 136 (2021) 18–27.
[60] B. Adhikari, N.A. Chowdhury, L.A. Diaz, H. Jin, A.K. Saha, M. Shi, J.R. Klaehn, T.E. Lister, Resour. Conserv. Recycl. 193 (2023) 106973.
[61] V. Agarwal, P.B. Zetterlund, Chem. Eng. J. 405 (2021) 127018.
[62] Q. Wei, S. Pei, G. Wen, K. Huang, Z. Wu, Z. Liu, W. Ma, H.M. Cheng, W. Ren, ACS Nano 13 (2019) 9482–9490.
[63] Z. Qiu, Z. Liu, J. Miao, F. Zheng, J. Jiang, Y. Li, Q. Wu, Y. Huang, H. Wang, Q. Li, Appl. Surf. Sci. 608 (2023) 155211.
[64] P.G. Schiavi, R. Zanoni, M. Branchi, C. Marcucci, C. Zamparelli, P. Altimari, M.A. Navarra, F. Pagnanelli, ACS Sustain. Chem. Eng. 9 (2021) 13303–13311.
[65] M. Lathika Divya, S. Natarajan, V. Aravindan, Batter Supercaps 2022 (2022) 202200046.
[66] Y. Zhang, N. Song, J. He, R. Chen, X. Li, Nano Lett. 19 (2019) 512–519.
[67] S. Ko, Y. Yamada, L. Lander, A. Yamada, Carbon 158 (2020) 766–771.
[68] X. Qi, B. Blizanac, A. DuPasquier, P. Meister, T. Placke, M. Oljaca, J. Li, M. Winter, PCCP 16 (2014) 25306–25313.
[69] M. Carboni, S. Brutti, A.G. Marrani, ACS Appl. Mater. Interfaces 7 (2015) 21751–21762.
[70] I. Ferrari, A. Motta, R. Zanoni, F.A. Scaramuzzo, F. Amato, E.A. Dalchiele, A.G. Marrani, Carbon 203 (2023) 29–38.